

Clumps and streams in the local dark matter distribution

J. Diemand¹, M. Kuhlen², P. Madau¹, M. Zemp¹, B. Moore³, D. Potter³, & J. Stadel³

¹*University of California, Department of Astronomy and Astrophysics, Santa Cruz, CA 95064, USA.*

²*Institute for Advanced Study, Einstein Drive, Princeton, NJ 08540, USA.*

³*University Zurich, Institute for Theoretical Physics, Winterthurerstrasse 190, 8057 Zurich, Switzerland.*

In cold dark matter cosmological models^{1,2}, structures form and grow by merging of smaller units³. Numerical simulations have shown that such merging is incomplete; the inner cores of halos survive and orbit as “subhalos” within their hosts^{4,5}. Here we report a simulation that resolves such substructure even in the very inner regions of the Galactic halo. We find hundreds of very concentrated dark matter clumps surviving near the solar circle, as well as numerous cold streams. The simulation reveals the fractal nature of dark matter clustering: Isolated halos and subhalos contain the same relative amount of substructure and both have cuspy inner density profiles. The inner mass and phase-space densities of subhalos match those of recently discovered faint, dark matter-dominated dwarf satellite galaxies^{6–8}, and the overall amount of substructure can explain the anomalous flux ratios seen in strong gravitational lenses^{9,10}. Subhalos boost gamma-ray production from dark matter annihilation, by factors of 4-15, relative to smooth galactic models. Local cosmic ray production is also enhanced, typically by a factor 1.4, but by more than a factor of ten in one percent of locations lying sufficiently close to a large subhalo. These estimates assume that gravitational effects of baryons on dark matter substructure are small.

The cold dark matter (CDM) model has been remarkably successful at describing the large-scale mass distribution of our Universe from the hot Big Bang to the present. However, the nature of the dark matter particle is best tested on small scales, where its interaction properties manifest themselves by modifying the structure of galaxy halos and their substructure. CDM theory predicts that the growth of cosmic structures begins early, on Earth mass scales^{11,12}, and continues from the bottom up until galaxy clusters form that are twenty orders of magnitude more massive. Resolving small-scale structures is extremely challenging, as the range of lengths, masses, and timescales that need to be simulated is immense. We have performed the highest precision calculation – dubbed “Via Lactea II” – of the assembly of the Galactic CDM halo. The simulation follows the growth of a Milky Way-size system in a Λ CDM Universe from redshift 104.3 to the present. It provides the most accurate predictions on the small scale clustering of dark matter and the first constraints on the local subhalo abundance and properties. We used the parallel treecode PKDGRAV2^[13] and sample the

galaxy-forming region with 1.1×10^9 particles of mass $4,100 M_\odot$. Cosmological parameters were taken from *WMAP* [14], see the online supplement for more details and a comparison to our previous Via Lactea simulation.

The wealth of substructure that survives the hierarchical assembly process to the present epoch is clearly seen in Figure 1: we resolve over 40,000 subhalos within 402 kpc of the center and they are distributed approximately with equal mass per decade of mass over the range $10^6 - 10^9 M_\odot$. They have very high central phase-space densities ($\gtrsim 10^{-5} M_\odot \text{pc}^{-3} \text{km}^{-3} \text{s}^3$) due to their steep inner density cusps and their relatively small internal velocity dispersions. This agrees well with the extremely high phase-space densities inferred from stellar motions within ultra faint dwarf galaxies⁷. Our predicted inner subhalo densities ($0.4 - 2.5 M_\odot \text{pc}^{-3}$ within 100 pc, $7 - 46 M_\odot \text{pc}^{-3}$ within 10 pc) are also in excellent agreement with the observations^{6,7}. The fact that CDM naturally predicts a small-scale dark matter distribution that matches the observations is a real success of the model. Particle candidates that introduce a low phase-space limit, such as a sterile neutrino, or that have a high collisional cross section such as self interacting dark matter would fail these fundamental observational tests.

The phase-space map (upper inset in Figure 1) also contains coherent elongated features. These are streams which form out of material removed from accreted and disrupted subhalos. The few visible streams have quite low densities (about 100 times below the local density) but owing to their low velocity dispersion (about 10 times smaller than that of background particles) they just barely manage to stand out in local phase space density (these streams have about $10^{-9} M_\odot \text{pc}^{-3} \text{km}^{-3} \text{s}^3$). These resolved streams together with the multitude of expected finer grained phase space structures that we currently can not resolve, will lead to unique signatures in direct detection experiments, especially those with directional sensitivity. In cases where the disrupted subhalo hosted a luminous satellite galaxy, the resulting streams would contain not only dark matter but also stars. This process would then produce detectable features in the Milky Way's stellar halo, like those observed in the "Field of Streams"¹⁵.

Further evidence for halo substructure comes from the anomalous flux ratios in multiply-imaged gravitationally lensed quasars^{16,17}. Perturbations to the light path from substructure can explain this phenomenon if the projected substructure fraction within 10 kpc is about one percent^{9,10}. Within a projected distance of 10 kpc from the center, 0.50% of the host mass belongs to resolved substructure, which could be just enough to explain the observed flux anomalies. In earlier simulations this fraction was lower, even the first Via Lactea halo¹⁸ had only 0.25% indicating that this quantity has not yet converged.

Via Lactea II predicts a remarkable self-similar pattern of clustering properties: Our simulation is the first to use an extremely accurate integration of particle orbits in high

density regions¹⁹, allowing a precise determination of the density profile within the inner kpc of the Galactic halo and within the centers of its satellite galaxies. We find that a cuspy profile fits the host halo density profile well, while the best fit cored profile lies below the simulated inner densities (Figure 2). The inner profiles of subhalos are also consistent with cusps over their resolved ranges. They scatter around the moderate cusp index of the host halo ($\gamma = 1.24$): Some of them are denser in the inner part, and some are less dense, exactly like the inner parts of *field* halos, which have inner slopes of $\gamma \simeq 1.2 \pm 0.2$ ^[20]. At large radii subhalo density profiles generally fall off faster than field halo profiles. These similarities and differences between subhalo and field halo profiles have a simple explanation: Subhalo density profiles were modified by tidal mass loss, which removes material from the outside in, but does not change the inner cusp structure^{18,21}. Figure 3 shows that the dwarf satellites of the Milky Way appear to be scaled versions of the main halo not just in their inner mass distribution, but also in term of relative substructure abundances. Via Lactea II demonstrates the fractal-like appearance of the dark matter by resolving the second generation of surviving sub-substructures from the merging hierarchy. This suggest that at infinite resolution one would find a long nested series of halos within halos within halos etc., reminiscent of a Russian Matryoshka doll, all the way down the first and smallest earth mass haloes that form.

The multitude of dark substructures increases the dark matter annihilation signal, since it is proportional to the *square* of the local density. For cuspy profiles (Figure 2) with some fixed inner slope ($\gamma < 1.5$) one gets the following simple scaling relation for the annihilation:

$$L \propto \rho_s^2 r_s^3 \propto V_{\max}^4 / r_{V\max} \propto V_{\max}^3 \sqrt{c_V}, \quad (1)$$

see the online supplement for the definition of the concentration c_V and its values. Combined with the steep subhalo velocity function $N(> V_{\max}) \propto V_{\max}^{-3}$, this implies that subhalos of all sizes contribute about equally to the total signal coming from the Galactic dark halo. Taking the higher concentrations of smaller systems²² into account, one finds that small subhalos are contributing more than large ones^{23,24}. Summing up $V_{\max}^4 / r_{V\max}$ of all resolved subhalos in Via Lactea II comes close (97%) to the host halo's $V_{\max}^4 / r_{V\max}$, i.e. the resolved subhalos already contribute as much as their smooth host alone would. In other words the "substructure boost factor" is at least 1.97. Extrapolating down to micro-subhalos of size $V_{\max} = 0.25 \text{ ms}^{-1}$, taking into account how concentrations depend on subhalo size²² and position (see the online supplement), and assuming a uniform distribution of subhalo inner slopes α between 1.0 and 1.5, leads to a total boost of 14.6. Most of it comes from very small clumps: halting the same extrapolation at $V_{\max} = 44 \text{ ms}^{-1}$ lowers the boost to 6.6. While the contribution from small, dark clumps itself is not affected by baryons, it may not dominate the total signal in scenarios in which baryonic collapse greatly increases the central dark matter densities in larger halos. However, the net effect of stars, black holes, and galaxy formation is unclear, and it may actually lead to a reduction in the central dark matter densities. The detailed distribution of cusp indices is still unknown, since only a few halos have been simulated with sufficient resolution²⁰. For the annihilation boost factors

the existence of a few steep cusps near 1.5 would make a big difference, since the signal diverges logarithmically towards the center in a $\gamma = 1.5$ cusp. Cutting the assumed uniform distribution of inner slopes at 1.4 instead of 1.5 gives a boost of 9.9 instead of 14.6, and 4.3 instead of 6.6. These factors imply that most of the extra-galactic γ -ray background from dark matter annihilation²³, which will be constrained or even detected by the upcoming GLAST mission, should be emitted by subhalos, and not by distinct host halos.

Besides γ -rays, dark matter annihilation would produce charged particles and anti-particles that, due to magnetic field entanglement, propagate over much smaller distances within the Galaxy. Space based experiments (like PAMELA, and in the near future AMS-02) could detect anti-particles produced in dark matter annihilations within about one kiloparsec²⁵. What fraction of this local annihilation would happen in nearby subhalos? To constrain this local boost factor we use the same assumptions as above ($\gamma = [1 - 1.5], V_{\max} \geq 0.25 \text{ m s}^{-1}$), but now we only include subhalos within one kiloparsec of the solar system (see the online supplement for the local subhalo abundance). The resulting signal is 40% of the smooth halo signal, giving a boost factor of 1.4, which we estimated using the spherically averaged density at 8 kpc ($\rho_0 = 0.40 \text{ GeV c}^{-2} \text{ cm}^{-3}$). Explaining the positron excess from the HEAT experiment²⁶ with local dark matter annihilation requires enhancements from about 3 to 100²⁵. When a relatively large subhalo happens to lie within 1 kpc, one can get the higher boost factors without violating the local subhalo constraints from our simulation. Such cases are possible, but not likely: Only 5.2 percent of all random realizations have a boost factor of 3 or larger (caused by a $V_{\max} \geq 3.4 \text{ km s}^{-1}$ clump within 1 kpc). In only 1.0 percent of the cases the boost factor reaches 10 or higher due to a nearby, large $V_{\max} \geq 5.6 \text{ km s}^{-1}$ subhalo.

1. Peebles, P. J. E. Large-scale background temperature and mass fluctuations due to scale-invariant primeval perturbations. *Astrophys. J. Lett.* **263**, L1–L5 (1982).
2. Blumenthal, G. R., Faber, S. M., Primack, J. R. & Rees, M. J. Formation of galaxies and large-scale structure with cold dark matter. *Nature* **311**, 517–525 (1984).
3. White, S. D. M. & Rees, M. J. Core condensation in heavy halos - A two-stage theory for galaxy formation and clustering. *Mon. Not. R. Astron. Soc.* **183**, 341–358 (1978).
4. Ghigna, S. *et al.* Dark matter haloes within clusters. *Mon. Not. R. Astron. Soc.* **300**, 146–162 (1998).
5. Klypin, A., Kravtsov, A. V., Valenzuela, O. & Prada, F. Where Are the Missing Galactic Satellites? *Astrophys. J.* **522**, 82–92 (1999).
6. Strigari, L. E. *et al.* The Most Dark Matter Dominated Galaxies: Predicted Gamma-ray Signals from the Faintest Milky Way Dwarfs. *Astrophys. J.* **678**, 624–620 (2008).
7. Simon, J. D. & Geha, M. The Kinematics of the Ultra-faint Milky Way Satellites: Solving the Missing Satellite Problem. *Astrophys. J.* **670**, 313–331 (2007).

8. Belokurov, V. *et al.* Cats and Dogs, Hair and a Hero: A Quintet of New Milky Way Companions. *Astrophys. J.* **654**, 897–906 (2007).
9. Dalal, N. & Kochanek, C. S. Direct Detection of Cold Dark Matter Substructure. *Astrophys. J.* **572**, 25–33 (2002).
10. Metcalf, R. B., Moustakas, L. A., Bunker, A. J. & Parry, I. R. Spectroscopic Gravitational Lensing and Limits on the Dark Matter Substructure in Q2237+0305. *Astrophys. J.* **607**, 43–59 (2004).
11. Green, A. M., Hofmann, S. & Schwarz, D. J. The power spectrum of SUSY-CDM on subgalactic scales. *Mon. Not. R. Astron. Soc.* **353**, L23–L27 (2004).
12. Diemand, J., Moore, B. & Stadel, J. Earth-mass dark-matter haloes as the first structures in the early Universe. *Nature* **433**, 389–391 (2005).
13. Stadel, J. G. Cosmological N-body simulations and their analysis. *PhD Thesis, University of Washington* (2001).
14. Spergel, D. N. *et al.* Three-Year Wilkinson Microwave Anisotropy Probe (WMAP) Observations: Implications for Cosmology. *Astrophys. J. Supp.* **170**, 377–408 (2007).
15. Belokurov, V. *et al.* The Field of Streams: Sagittarius and Its Siblings. *Astrophys. J. Lett.* **642**, L137–L140 (2006).
16. Mao, S. & Schneider, P. Evidence for substructure in lens galaxies? *Mon. Not. R. Astron. Soc.* **295**, 587–+ (1998).
17. Metcalf, R. B. & Madau, P. Compound Gravitational Lensing as a Probe of Dark Matter Substructure within Galaxy Halos. *Astrophys. J.* **563**, 9–20 (2001).
18. Diemand, J., Kuhlen, M. & Madau, P. Formation and Evolution of Galaxy Dark Matter Halos and Their Substructure. *Astrophys. J.* **667**, 859–877 (2007).
19. Zemp, M., Stadel, J., Moore, B. & Carollo, C. M. An optimum time-stepping scheme for N-body simulations. *Mon. Not. R. Astron. Soc.* **376**, 273–286 (2007).
20. Diemand, J., Moore, B. & Stadel, J. Convergence and scatter of cluster density profiles. *Mon. Not. R. Astron. Soc.* **353**, 624–632 (2004).
21. Kazantzidis, S. *et al.* Density Profiles of Cold Dark Matter Substructure: Implications for the Missing-Satellites Problem. *Astrophys. J.* **608**, 663–679 (2004).
22. Bullock, J. S. *et al.* Profiles of dark haloes: evolution, scatter and environment. *Mon. Not. R. Astron. Soc.* **321**, 559–575 (2001).
23. Ullio, P., Bergström, L., Edsjö, J. & Lacey, C. Cosmological dark matter annihilations into γ rays: A closer look. *Phys. Rev. D* **66**, 123502–+ (2002).

24. Colafrancesco, S., Profumo, S. & Ullio, P. Multi-frequency analysis of neutralino dark matter annihilations in the Coma cluster. *Astron. & Astrophys.* **455**, 21–43 (2006).
25. Lavallo, J., Yuan, Q., Maurin, D. & Bi, X. . Full Calculation of Clumpiness Boost factors for Antimatter Cosmic Rays in the light of Λ CDM N-body simulation results. *Astron. & Astrophys.* **479**, 427–452 (2008).
26. Beatty, J. J. *et al.* New Measurement of the Cosmic-Ray Positron Fraction from 5 to 15GeV. *Physical Review Letters* **93**, 241102–+ (2004).
27. Sharma, S. & Steinmetz, M. Multidimensional density estimation and phase-space structure of dark matter haloes. *Mon. Not. R. Astron. Soc.* **373**, 1293–1307 (2006).
28. Bertschinger, E. Multiscale Gaussian Random Fields and Their Application to Cosmological Simulations. *Astrophys. J. Supp.* **137**, 1–20 (2001).
29. Navarro, J. F. *et al.* The inner structure of Λ CDM haloes - III. Universality and asymptotic slopes. *Mon. Not. R. Astron. Soc.* **349**, 1039–1051 (2004).
30. Reed, D. *et al.* Dark matter subhaloes in numerical simulations. *Mon. Not. R. Astron. Soc.* **359**, 1537–1548 (2005).

Supplementary Information is linked to the online version of the paper at www.nature.com/nature.

Acknowledgements It is a pleasure to thank Bronson Messer and the Scientific Computing Group at the National Center for Computational Sciences for their help. The “Via Lactea II” simulation was performed at the Oak Ridge National Laboratory through an award from DOE’s Office of Science as part of the 2007 Innovative and Novel Computational Impact on Theory and Experiment (INCITE) program. Additional computations (initial conditions generation, code optimisations and smaller test runs) were carried out on the MareNostrum supercomputer at the BSC, on Columbia at NASA Ames and on the UCSC Astrophysics Supercomputer Pleiades. This work was supported by NASA and the Swiss National Science Foundation.

Competing Interests The authors declare that they have no competing financial interests.

Correspondence Correspondence and requests for materials should be addressed to J. D. (email: diemand@ucolick.org).

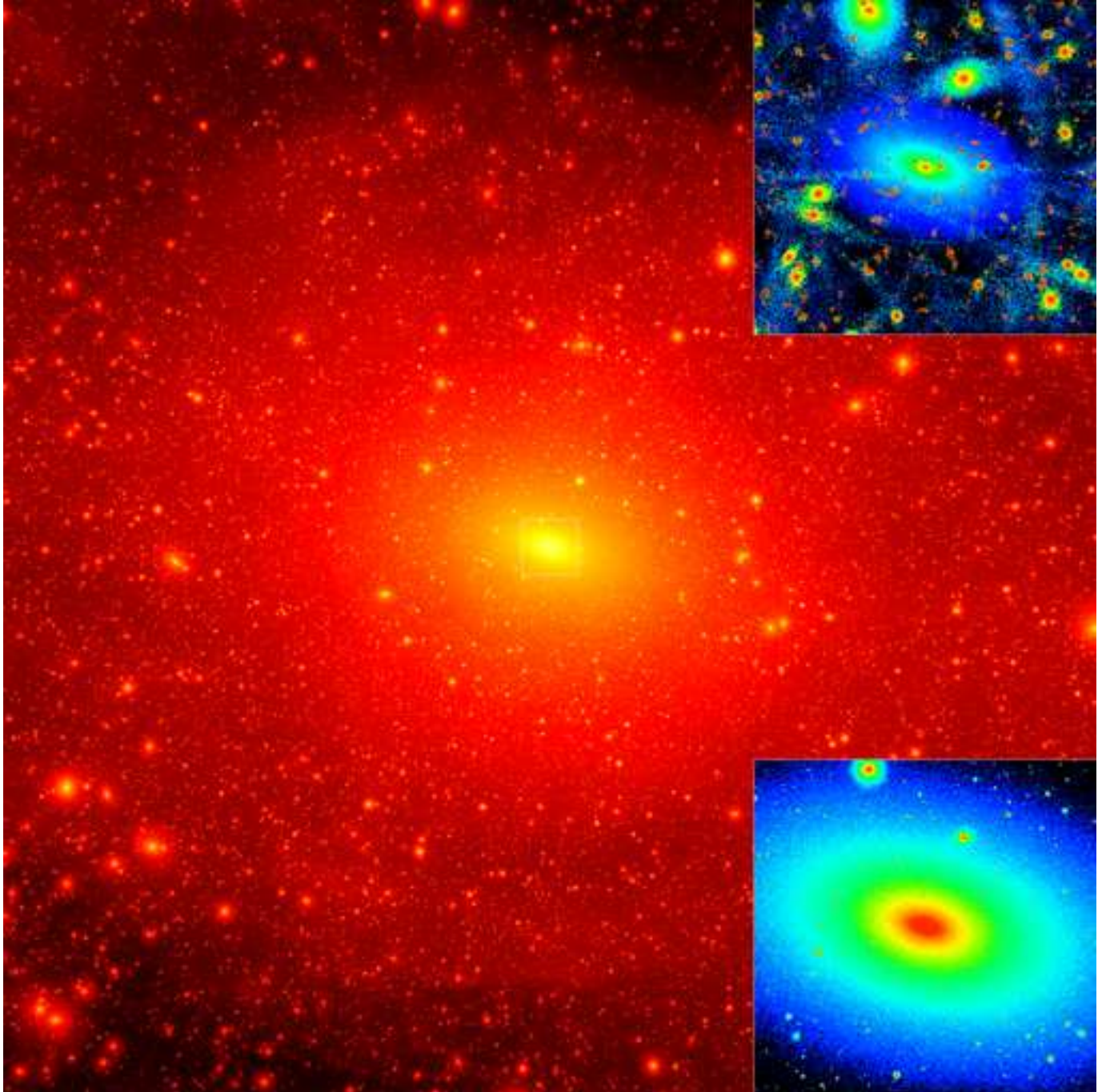


Figure 1: Projected dark matter density-square map of “Via Lactea II”. An 800 kpc cube is shown. The insets focus on an inner 40 kpc cube, in local density (bottom), and in local phase space density calculated with EnBiD^[27] (top). The Via Lactea II simulation has a mass resolution of $4,100 M_{\odot}$ and a force resolution of 40 pc. It used over a million processor hours on the “Jaguar” Cray XT3 supercomputer at the Oak Ridge National Laboratory. A new method was employed to assign physical, adaptive time-steps¹⁹ equal to 1/16 of the local dynamical timescale (but not shorter than 268,000 yr), which allows to resolve very high density regions. Initial conditions were generated with a modified, parallel version of GRAFIC2^[28]. The high resolution region is embedded within a large periodic box (40 comoving Mpc) to account for the large scale tidal forces. The mass within 402 kpc (the radius enclosing 200 times the mean matter density) is $1.9 \times 10^{12} M_{\odot}$.

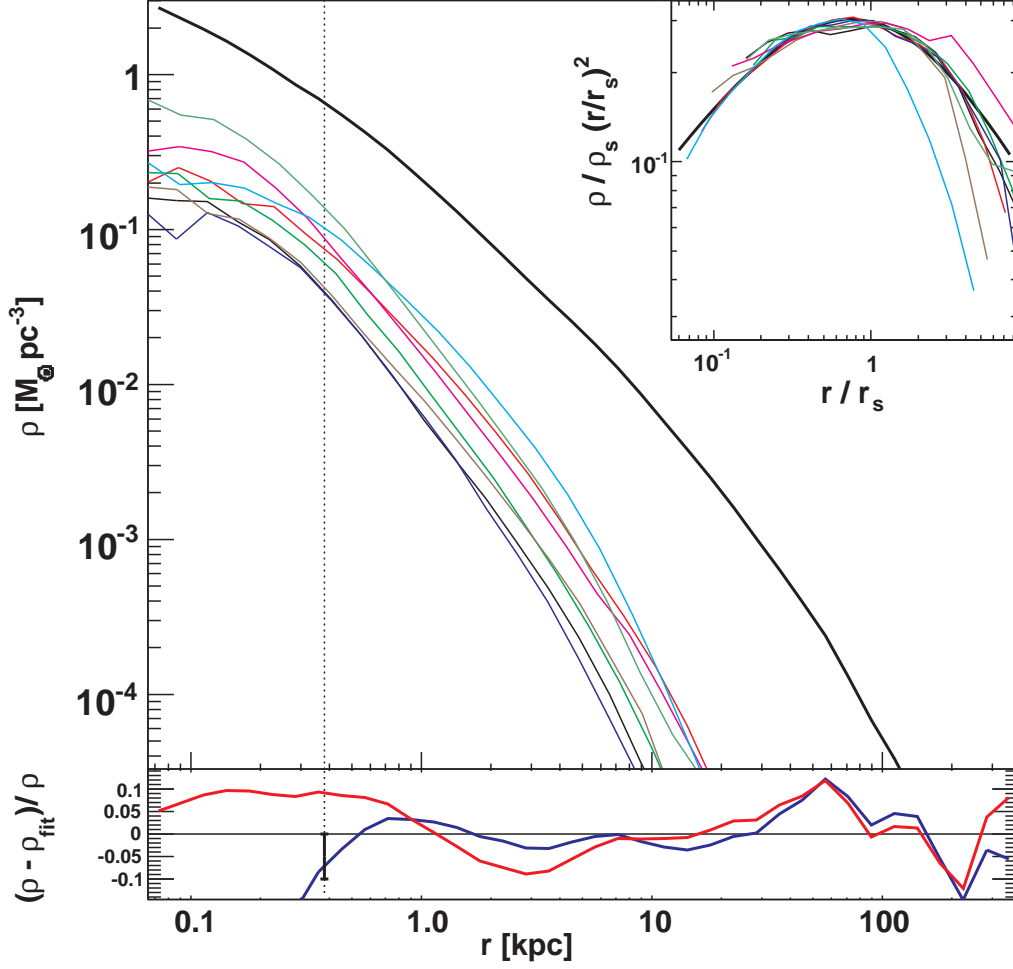


Figure 2: Density profiles of main halo and subhalos. *Main panel:* Profile of the Milky Way halo (*thick line*) and of eight large subhalos (*thin lines*). The *lower panel* gives the relative differences between the simulated main halo profile and a fitting formula with a core²⁹ $\rho(r) = \rho_s \exp\{-2/\alpha [(r/r_s)^\alpha - 1]\}$, with best fit parameters: $\alpha = 0.170$, $r_s = 21.5$ kpc, $\rho_s = 1.73 \times 10^{-3} M_\odot \text{pc}^{-3}$ (*red curve*) and one with a cusp²⁰ $\rho(r) = \rho_s (r/r_s)^{-\gamma} (r/r_s + 1)^{-3+\gamma}$ with a best fit inner slope of $\gamma = 1.24$, $r_s = 28.1$ kpc, $\rho_s = 3.50 \times 10^{-3} M_\odot \text{pc}^{-3}$ (*blue curve*). The vertical dotted line indicates the estimated convergence radius of 380 pc: simulated local densities are only lower limits inside of 380 pc and they should be correct to within 10% outside this region. The cuspy profile is a good fit to the inner halo, while the cored profile has a too shallow slope in the inner few kpc, causing it to overestimate densities around 4 kpc and to underestimate them at all radii smaller than 1 kpc. The simulated densities are higher than the best fit cored profile even at 80 pc, where they are certainly underestimated due to numerical limitations. We find the same behavior in the inner few kpc in all six snapshots we have analyzed so far between $z=3$ and $z=0$. The large residuals in the outer halos on the other hand are transient features, they are different in every snapshot. *Inset:* Rescaled host (*thick line*) and subhalo (*thin lines*) density profiles multiplied by radius square to reduce the vertical range of the figure.

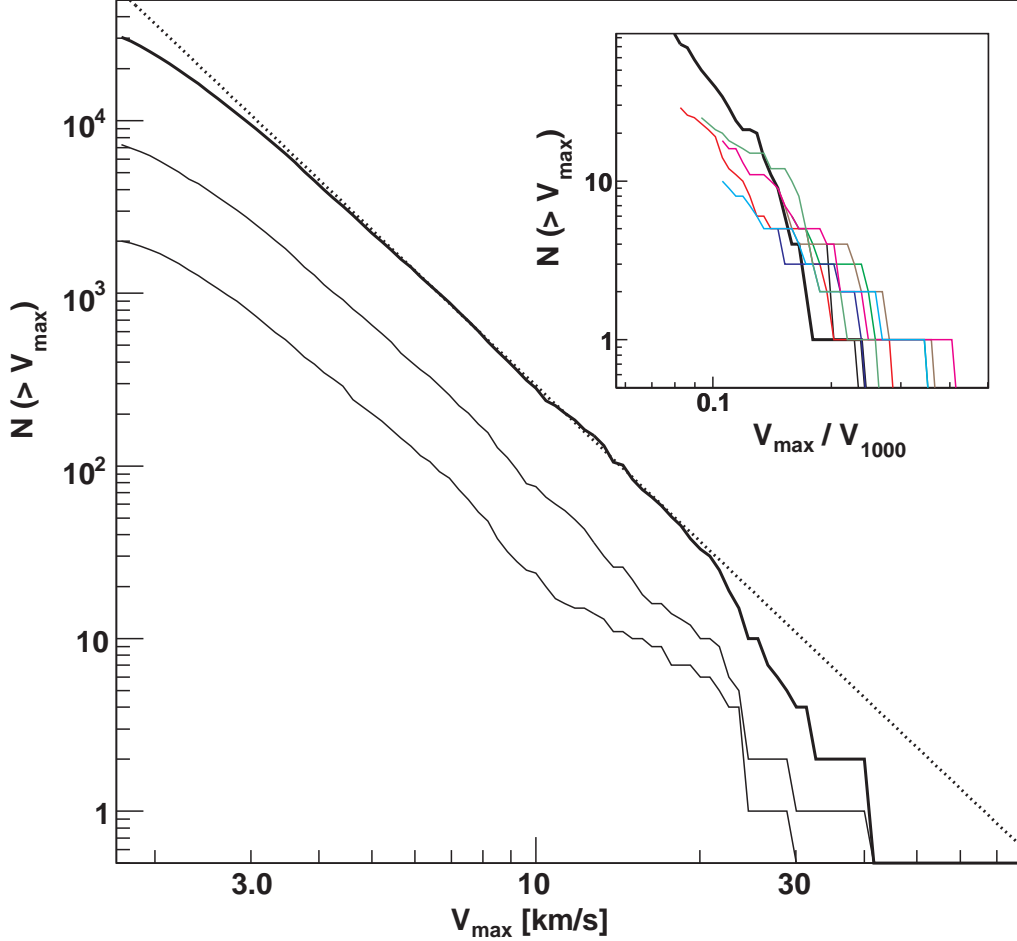


Figure 3: Subhalo and sub-subhalo abundances. Number of subhalos above V_{\max} within $r_{200} = 402$ kpc (thick solid lines) and within 100 and 50 kpc of the galactic center (thin solid lines). V_{\max} is the peak height of the subhalo circular velocity $v_{\text{circ}} = \sqrt{GM(< r)/r}$ and serves as a simple proxy for the mass of a subhalo. The dotted line is $N(> V_{\max}) = 0.036 (V_{\max}/V_{\max,\text{host}})^{-3}$, where $V_{\max,\text{host}} = 201 \text{ km s}^{-1}$ (at $r_{V_{\max,\text{host}}} = 60$ kpc). It fits the subhalo abundance above $V_{\max} \simeq 3.5 \text{ km s}^{-1}$. The number of smaller subhalos is artificially reduced by numerical limitations. Inside r_{200} this halo has 1.7 times more substructure than the first Via Lactea halo¹⁸, a factor well within the halo-to-halo scatter³⁰. Inside 50 kpc the difference grows to 2.6, probably due to the improved mass and time resolution of Via Lactea II, which allows to resolve inner substructure better. The *inset* shows the sub-subhalo abundance within r_{1000} (enclosing 1000 times the mean matter density) of the centers of eight (same ones as in Fig. 2) large subhalos (thin solid lines). r_{1000} is well inside of the tidal radius for these systems. The thick solid line shows the subhalo abundance of the host halo inside of its $r_{1000} = 213$ kpc. The (sub-)subhalo V_{\max} values are given in units of $V_{1000} = \sqrt{GM(< r_{1000})/r_{1000}}$ of the corresponding host (sub-)halo. Lines stop at $V_{\max} = 2 \text{ km s}^{-1}$. The mean sub-substructure abundance is consistent with the scaled down version of main halo, and both the mean abundance and the scatter agree with results in³⁰ for distinct *field* halos.

Supplementary Notes

In this Supplementary Information, we give more details about the Via Lactea II (VL-II) simulation presented in our Letter. The first part provides additional results about radial trends in subhalo abundance and properties. In the second part we include some comparisons with the Via Lactea (VL-I) run, previously the largest simulation of the Galactic dark matter halo.

Supplementary Figure 1 illustrates how tidal interactions with the gravitational potential of the host shape the radial distribution of subhalos and their internal structure. Tides remove mass from the outer parts of subhalos. Clumps closer to the Galactic center lose more mass as they experience stronger tidal forces and more pericenter passages¹⁸. Mass loss also reduces V_{\max} and $r_{V_{\max}}$, which leads to an increase in $\bar{\rho}(< r_{V_{\max}})$. The radial distribution of subhalos with $V_{\max} > 3 \text{ km s}^{-1}$ is more extended than the dark matter distribution in the Galactic halo, a feature that does not depend on subhalo size, i.e. different V_{\max} selection thresholds lead to the same radial distribution. VL-II resolves subhalos as close as 8 kpc from the Galactic center, but it is possible that it underestimates the true substructure abundance inside 20 kpc due to numerical limitations. Subhalo concentrations are defined as the mean density within $r_{V_{\max}}$, the radius of peak circular velocity, a quantity that is well determined both for isolated halos and subhalos and does not depend on assumptions about their density profiles¹⁸:

$$c_V \equiv \bar{\rho}(< r_{V_{\max}})/\rho_{\text{crit},0} = (V_{\max}/r_{V_{\max}})^2 4\pi/(3G\rho_{\text{crit},0}), \quad (2)$$

where $\rho_{\text{crit},0} = 1.48 \times 10^{-7} \text{ M}_{\odot} \text{ pc}^{-3}$. The median subhalo concentration increases strongly towards the Galactic center, both because of tidal mass losses and to a lesser extent because of the earlier formation times of inner substructure¹⁸.

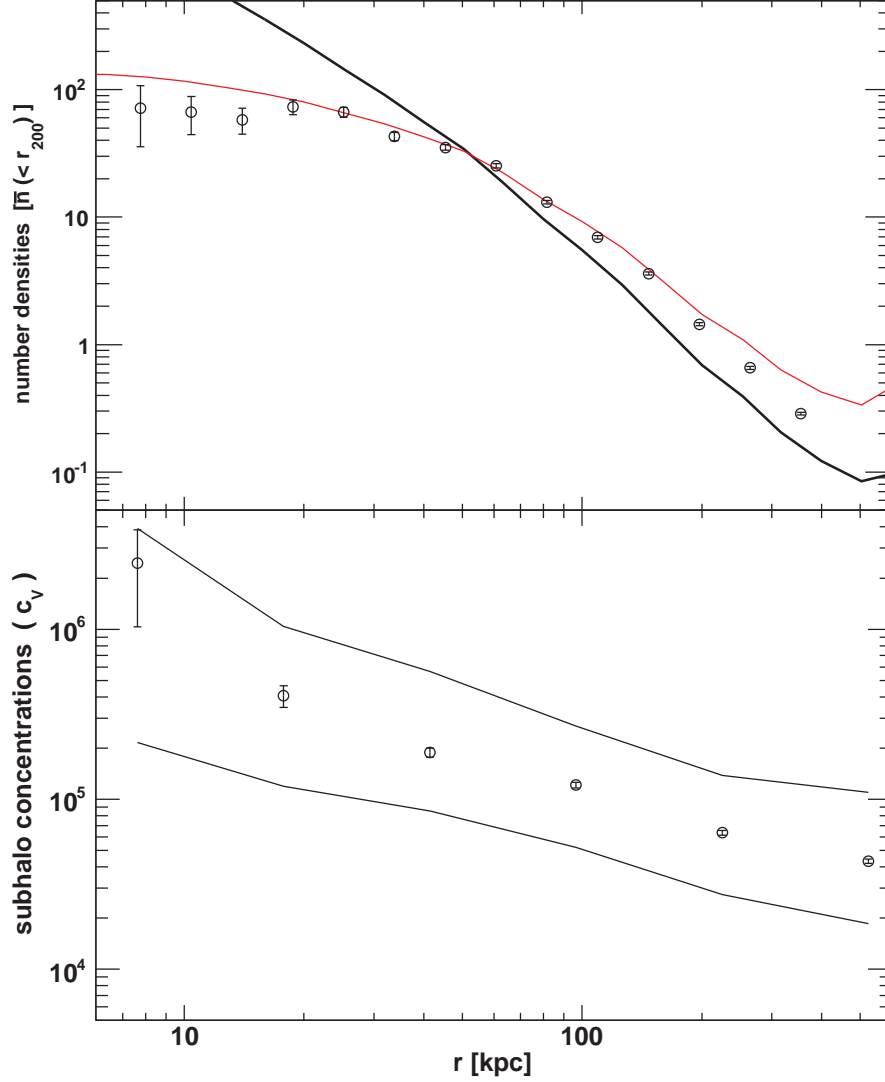
Supplementary Table 1 summarises the numerical parameters and host halo properties of the VL-I and VL-II simulations. The main difference between these runs is the improved time stepping in VL-II, which at each time and for each particle is based on the local dynamical time $\sqrt{1/G\rho_{\text{enc}}}$ ^[19], where ρ_{enc} is the mean density enclosed in a sphere extending out to the particle's position and centered on the dynamically dominant structure. In VL-I we adopted instead the standard ad-hoc time-step criterion based on the acceleration and the gravitational softening of the particle ($\propto \sqrt{\epsilon/|\mathbf{a}|}$). This criterion fails in high density regions and artificially flattens the inner cuspy halo density profiles³¹. This limitation set the convergence radius of VL-I (where the host true density profile is reproduced to within 10 percent) to $r_{\text{conv}} = 1.3 \text{ kpc}$. The new time stepping used in VL-II allows us to properly resolve the host density profile on significantly smaller scales: the finite mass resolution determines a convergence radius²⁰ of about 0.38 kpc for VL-II. The VL-I subhalo density profiles are also affected by this limitation: the enclosed densities within 300 pc of large subhalos are about twice as high in VL-II. Further out, at 600 pc, the enclosed subhalo densities are very similar in VL-I and VL-II.

To check for numerical convergence and test the dependence of our results on numerical and cosmological parameters we ran a series of lower resolution versions of VL-II. The mass resolution in this "VL-II_m" series is 64 times coarser and the force softening length 4 times larger than in VL-II. Supplementary Figure 2 shows that the lower resolution version of the same halo has a very similar subhalo velocity function above about $0.05 V_{\text{max,host}} \simeq 10 \text{ km s}^{-1}$. Rescaling to 64 times less massive systems suggests that VL-II should have converged down to about 2.5 km s^{-1} , which indeed is close to the scale where the VL-II velocity function starts to fall below the power law fit (Figure 3). The earlier starting redshift of VL-II does not seem to affect the $z = 0$ substructure abundance significantly. We find only a weak dependence on cosmological parameters: VL-II used the best fit Λ CDM parameters from the *WMAP* 3 year data release¹⁴: $\Omega_m = 0.238$, $\Omega_\Lambda = 0.762$, $h=0.73$, $n_s=0.951$, and $\sigma_8=0.74$. For comparison we have ran a simulation with *WMAP* 1 year parameters³²: $\Omega_m = 0.27$, $\Omega_\Lambda = 0.73$, $h=0.72$, $n_s=1.0$, and $\sigma_8=0.9$. The higher σ_8 and steeper spectral index n_s in *WMAP1* lead to more small scale power. The effect on the $z = 0$ substructure abundance is rather small: our WMAP1 run has about 20 to 30 percent more subhalos relative to the WMAP3 runs, in agreement with semi-analytical predictions (see Figure 11 in³³).

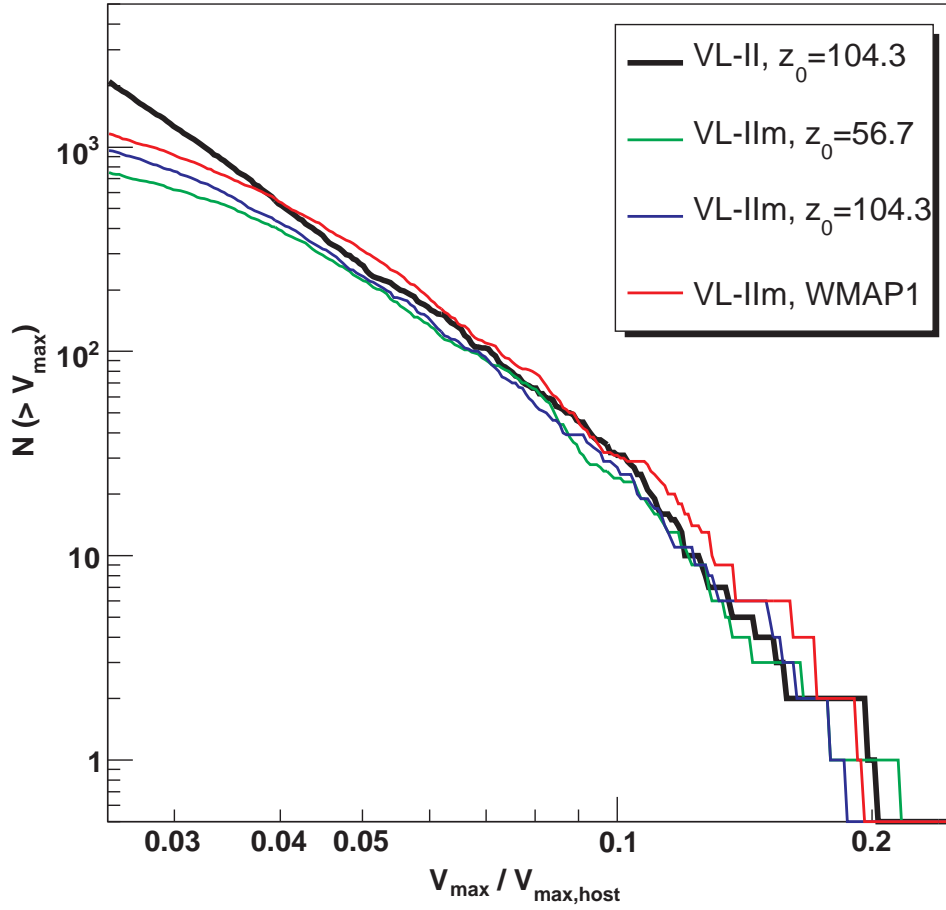
31. Diemand, J., Zemp, M., Stadel, J., Moore, B. & Carollo, C. M. Cusps in cold dark matter haloes. *Mon. Not. R. Astron. Soc.* 364, 665–673 (2005).

32. Spergel, D. N. et al. First-Year Wilkinson Microwave Anisotropy Probe (WMAP) Observations: Determination of Cosmological Parameters. *Astrophys. J. Supp.* 148, 175–194 (2003).

33. Zentner, A. R. & Bullock, J. S. Halo Substructure and the Power Spectrum. *Astrophys. J.* 598, 49–72 (2003).



Supplementary Figure 4: Abundance and concentrations of subhalos vs. distance from the galactic center. *Top:* The number density profile of subhalos (circles) is more extended than the dark matter density profile $\rho(r)$ (thick line). Their ratio turns out to be roughly proportional to the enclosed mass $M(< r)$, i.e. $\rho M(< r)$ (thin line) matches the subhalo number density quite well. Only subhalos larger than $V_{\text{max}} = 3 \text{ km s}^{-1}$ are included here. *Bottom:* Subhalo concentrations (median and 68% range are shown) increase towards the center, where the stronger tidal force remove more of the outer, low density parts from the subhalos. To make sure their c_V are resolved, only subhalos larger than $V_{\text{max}} = 5 \text{ km s}^{-1}$ are used. The error bars indicate the statistical uncertainties in both panels.



Supplementary Figure 5: Subhalo abundance at different numerical resolutions, starting redshifts and cosmologies. Number of subhalos above $V_{\max}/V_{\max, \text{host}}$ within r_{200} for the VL-II simulation and three lower resolution versions of the same halo.

Name	ΔT	ϵ (pc)	z_i	r_{conv} (kpc)	M_{hires} (M_{\odot})	r_{200} (kpc)	M_{200} (M_{\odot})	V_{max} (km s^{-1})	$r_{V_{\text{max}}}$ (kpc)
VL-I	$0.2\sqrt{\epsilon/ \mathbf{a} }$	90.0	48.4	1.3	2.1×10^4	389	1.77×10^{12}	181	69
VL-II	$0.06\sqrt{1/G\rho_{\text{enc}}}$	40.0	104.3	0.38	4.1×10^3	402	1.93×10^{12}	201	60

Supplementary Table 1: Simulation parameters and halo properties. Time step criterion ΔT , spline force softening length ϵ , initial redshift z_i , convergence radius of the host halo density profile r_{conv} , mass M_{hires} of high resolution dark matter particles and host halo r_{200} , M_{200} , V_{max} and $r_{V_{\text{max}}}$ for the VL-I and VL-II simulations. At each time individual particle time steps are chosen by dividing the base time step of 13.7 Gyr / 400 by two until it is smaller than ΔT , where $|a|$ is the norm of the acceleration vector and ρ_{enc} is the enclosed density within the dynamically dominant structure. Force softening lengths ϵ are constant in physical units back to $z = 9$ and constant in comoving units before.